



Retention During Freezing of Raindrops, Part II: Investigation of Ambient Organics from Beijing Urban Aerosol Samples

Jackson Seymore*¹, Martanda Gautam¹, Miklós Szakáll¹, Alexander Theis², Thorsten Hoffmann², Jialiang Ma³, Lingli Zhou⁴, Alexander L. Vogel³

5 ¹ Institute for Atmospheric Physics, Johannes Gutenberg University, Mainz, Germany

² Particle Chemistry Department, Max Planck Institute for Chemistry, Mainz, Germany

³ Institute for Atmospheric and Environmental Sciences, Goethe University Frankfurt, Germany

⁴ South China Institute of Environmental Sciences, Ministry of Ecology and Environment, Guangzhou, P.R. China

*Corresponding author: seymorej@uni-mainz.de

10 **Keywords:** retention, dissolved organic matter, DOM, Orbitrap MS, secondary organic aerosol, SOA, convective clouds, acoustic levitator

Abstract

The freezing of hydrometeors incurs certain water-soluble organic compounds dissolved in the supercooled cloud droplets to be released into the gas phase. This may lead to the vertical redistribution of substances that become available for new particle formation in the upper troposphere. Drop freezing experiments were performed on the Mainz Acoustic Levitator (M-AL) using aqueous extracts of ambient samples of Beijing urban aerosol. The retention coefficients of over 450 compounds were determined. Most nitroaromatics and organosulfates were fully retained along with the aliphatic amines (AA) and higher-order amines and amides while sulfides, lipids, aromatic hydrocarbons, and long chain compounds are among the most unretained and incidentally the fewest species observed. The findings here also indicate that NO_x and SO_x chemistry, particularly anthropogenically related, enhances the retention of the resulting secondary organic aerosols (SOA). A positive correlation between polarity and freezing retention along with a negative correlation with vapor pressure and freezing retention was observed. No sigmoidal relationship with effective Henry's law constant was observed which differs with the parameterizations of riming retention presented in current literature, which is justified by the lower surface-to-volume ratio of the large drop size investigated.

15
20
25



1 Introduction

Atmospheric organic matter (OM) plays a critical role in climate regulation directly through radiation scattering and indirectly through cloud condensation nucleation which impacts Earth's energy balance through radiative forcing (Fofie et al., 2018; Liu et al., 2018). These effects are controlled by factors such as their optical properties, size, and the hygroscopicity (Dusek et al., 2006; Sun et al., 2021), which can change based on the proportions of primary organic aerosols (POA)—directly emitted aerosols—and secondary organic aerosols (SOA)—aerosols formed from the oxidation products of volatile organic compounds (VOC) as part of new particle formation (NPF) (Hallquist et al., 2009; Liu et al., 2021; Riva et al., 2019). Convective systems have been suggested to support NPF in the outflow region by reducing existing particle concentrations, facilitating cold temperatures, and transporting reactive gases into regions with high actinic fluxes (Clarke et al., 1998; Zheng et al., 2021)

Nucleation-mode particles—with sizes in the lower tens of nm—have consistently been observed in concentrations of up to 10^4 cm^{-3} from aircraft in the upper troposphere (Andreae et al., 2018; Andrés Casquero-Vera et al., 2020; Clarke et al., 1999; Heitto et al., 2024; Weigel et al., 2011; Williamson et al., 2019). These measurements significantly exceed the corresponding concentrations in the planetary boundary layer and indicate that the main source of such ultra-fine particles in the upper troposphere is in situ NPF rather than their direct transport from the boundary layer (Bardakov et al., 2021). The traditional explanation for this phenomenon has been that the reduction of existing aerosol particles in deep convective clouds eliminates removal processes for small particles and condensable vapors, supporting NPF (Clarke et al., 1998). However, Williamson et al. (2019) also showed that even without these conditions, such as in tropical convection, these newly formed particles can still be found. They then argue that most models underestimate available organic matter at high altitudes and as a result predict less NPF in these regions. If this NPF is the result of an overlooked mechanism of organic matter transport, it is then critical to elucidate this mechanism so to constrain uncertainty around the influence of high altitude NPF from convective outflows (Bardakov et al., 2021).



Publications by Borchers et al. (2024) and Jost et al., (2017) have demonstrated a potential mechanism for organic matter transport in mixed-phase clouds. They describe how organic compounds that are exchanged between the gas and aqueous phase in cloud droplets can either be trapped in the ice phase during freezing—washing them out by precipitation—or return to the gas phase by volatilization. This revolatilization incurred by the freezing process leads to a vertical redistribution and has the potential to explain the occurrence of organic matter at high altitudes in regions with deep convection. Alternatively, earlier publications by Pruppacher and Klett (2010) and Snider and Huang (1998) have suggested that complete sublimation of ice particles can also transport ‘retained’ compounds trapped in the ice phase and release them at high altitudes.

In convective clouds the main formation pathway of precipitation-size ice particles is riming, i.e. the freezing of supercooled μm -sized cloud droplets on the surface of a mm-sized ice particle. Thus, riming retention is an important process for the vertical redistribution of water-soluble organic compounds (WSOC). Convective clouds with warm bases favor the formation of mm-sized drops by collision-coalescence (Lamb and Verlinde, 2011), which subsequently can be uplifted in the updraft to regions with temperatures below 0°C . Once beyond the freezing level they can freeze and thereby release dissolved matter into the gas phase. This identifies freezing retention of mm-sized drops as a potential contributor to the vertical redistribution of WSOCs and was experimentally investigated in the present study.

The proportion of a substance that remains in the ice during this phase change is described by the retention coefficient R , which indicates the percentage of the trapped substance with a value between 0 and 1 (Bela et al., 2018; Iribarne and Pyshnov, 1990; Snider et al., 1992; Stuart and Jacobson, 2004). A species’ retention is influenced by its chemical properties, such as its dimensionless effective Henry’s law solubility constant (H^*), as well as the physical properties of the droplet such as temperature, liquid water content, droplet size, and ventilation. Substances with a small H^* are more likely to return to the gas phase during riming, which results in a lower retention coefficient. Additionally, these external and



physical conditions of the droplet disproportionately influence the retention for these small H* substances (Jost et al., 2017; Stuart and Jacobson, 2003, 2004)

Current experimental studies to determine retention coefficients for atmospheric constituents and relevant SOA precursors have focused on inorganic species, small organics, or single component mixtures with significantly higher than natural concentrations. Additionally, current studies have only examined retention in droplets within natural cloud size range rather than raindrop sizes. The few studies that look at complex mixtures are limited to compounds of similar families and only a handful of species (Borchers et al., 2024). Naturally occurring atmospheric constituents that are observed in rainwater are present as complex mixtures of potentially thousands of species (Seymore et al., 2023). To get closer to observing the retention of compounds in their natural conditions, this study presents measurements of retention coefficients for a real, complex mixture of WSOC extracted from filter samples taken in an urban environment.

2 Methods

2.1 Sampling Location and Method

A high-volume sampler (HiVol) was run with quartz fiber TSP filters over three nights between March 3 and 5, 2022 in Beijing, China (40.0426° N, 116.4197° E) for an approximate sample volume of 550 m³ between the hours of 21:00 to 9:00. These filters were sealed in aluminum foil and stored at -20°C until analysis. Aqueous extracts of these filters were prepared by taking 1/4 of each filter, combining them (in total 3/4 of a 203 x 254 mm filter area) in 30 ml Milli-Q water, and then extracting with an orbital shaker for 15 min. The same was performed for a blank sample; a total 3/4 of unsampled filter area was extracted in 30 ml Milli-Q water for 15 min. These extracts were filtered through a 0.2 µm PTFE filter. 10 ml of the prepared extract was reserved for Ultra-High Performance Liquid Chromatography High-



100 Resolution Orbitrap Mass Spectrometry (UHPLC-HRMS) analysis and stored at 3 °C while the remaining
20 ml was sent to Institute for Atmospheric Physics at the Johannes Gutenberg University of Mainz,
Germany for freezing experiments.

2.2 Mainz Acoustic Levitator (M-AL)

105 Freezing experiments were performed in an acoustic levitator (APOS BA 10, tec5 GmbH). This
allows contact-free single-drop levitation maintained by a standing ultrasonic wave. This setup and its
relevant physical influences are described in detail by Diehl et al., (2014), Szakáll et al., (2021), and in
part 1 of this publication series by Gautam et al. (2024). For the freezing experiment, the M-AL is placed
inside a walk-in cold room where the ambient temperature was set to -15°C. The M-AL is surrounded by a
110 protective acrylic housing to prevent any disturbance from air motion which may cause unsteady
temperature conditions, unstable levitation, or carry unwanted ice-nucleating particles onto the drop
surface. Air temperature in the M-AL was measured by a PT100 sensor and an infrared thermometer (KT
19.82 II, Heitronics) was used to monitor drop surface temperature.

The aqueous filter extract was injected with a syringe into the M-AL node to form a single free-
115 floating drop with a diameter of 2 ± 0.1 mm. The drop was allowed to freeze without the introduction of
artificial freezing nucleator. Freezing time was approximately 90 seconds on average but not longer than 3
min. Once the drop was fully frozen, it was removed from the M-AL and stored in a
polytetrafluoroethylene (PTFE) vial at -20°C until analysis. Enough drop to reach the minimum viable
sample volume for analysis, 50 µl, were collected to produce a single sample (approximately 12 drops).
120 Two full samples were collected for UHPLC-HRMS analysis. The blank filter extract was also used in the
freezing experiment to produce two more travel blank samples for comparative analysis and background
subtraction.



2.3 UHPLC-HRMS analysis

125 In addition to the M-AL frozen extract and the travel blanks, 100 μ l of the reserved extract and
Milli-Q solvent was analyzed by UHPLC-HRMS. Chromatographic separation was performed (Vanquish
Flex, Thermo Fisher Scientific Inc.) on a reversed phase column (Cortecs Solid Core T3, 2.7 μ m, 150 \times 3
mm, with the corresponding VanGuard Cartridge, Waters Corp.). Samples were ionized in negative and
positive mode using a heated electrospray ionization source (HESI-II Probe, Thermo Fisher Scientific
130 Inc.) and then detected with a high-resolution hybrid quadrupole-Orbitrap mass spectrometer (Q Exactive
Focus, Thermo Fisher Scientific Inc.). The chromatographic settings and gradient are as follows: LC
solvent A: ultrapure water with 0.1% formic acid; LC solvent B: methanol with 0.1% formic acid; Flow
rate 400 μ l min^{-1} ; pre-column heater and post-column cooler 40 $^{\circ}$ C; Gradient: 0 min 1% B; 1 min 1% B;
15 min 99% B; 16.5 min 99% B; 17.5 min 1% B; 20 min 1% B. The MS settings were at fullMS scan
135 (m/z 50-750; resolution 70k) along with data-dependent MS2 in discovery mode (resolution at 17.5k) for
acquiring fragmentation spectra of the largest peaks.

2.4 Non-targeted Analysis and Property Estimation

Compound identification confidence is communicated here using the convention described in
140 Schymanski et al., (2014). The raw UHPLC-HRMS files were processed on Compound Discoverer 3.3
(Thermo Fisher Scientific). This software aligned chromatographic peaks of interest with a maximum
shift of 0.1 min in retention time and a mass tolerance of ± 2 ppm. Mass traces with retention times less
than 1.8 min were excluded as they are not considered to be chromatographically separated. Ions were
detected if the peak intensity was at least 5×10^5 counts for $[M-H]^-$ for negative mode or $[M+H]^+$ and
145 $[M+Na]^+$ for positive mode. In addition to the mass-to-charge ratio of the detected ion, at least one
corresponding isotopologue had to be measured. The tolerance between the measured and calculated
intensity of the isotopologue was less than 30 %. These unknown compounds were then grouped with a



retention time tolerance of 0.1 min to produce a merged MS feature and those of them with a sample-to-blank ratio smaller than 5 were marked as background and removed from the dataset. Any compounds that did not appear in the reserved sample of filter extract were also removed from the dataset. A peak quality score was given on a scale of 0 to 10—with 10 being a perfect chromatographic peak—for each mass trace based on its peak shape qualities, e.g. peak jaggedness, modality. For all mass traces with a peak quality higher than 6 in all samples, a predicted composition for each mass trace was calculated within ± 2 ppm with the allowed elements of carbon (C), hydrogen (H), nitrogen (N), oxygen (O), and sulfur (S). Compounds were grouped together as CHO, CHNO, CHOS, and CHNOS. It is important to note that phosphorus (P) containing species were not considered for this study. All level 5 (L5) or higher compounds including any mass traces that did not fit a predicted composition within ± 2 ppm were used for calculating retention coefficients using their integrated MS signals. Level 4 (L4) or higher compounds with determined compositions were used for Van Krevelen and Kroll analysis to highlight the validity of the dataset as a real, complex mixture of urban-influenced WSOC. To aid the visualization of MS data, a Van Krevelen diagram cross-plots the H:C ratio as a function of the O:C ratio while a Kroll diagram cross-plots the estimated average carbon oxidation state as a function of the number of carbon atoms. An estimated vapor pressure at 298 K was then calculated for the elemental composition based on the parameterization by Li et al. (2016).

The predicted compound list was then matched against the mzCloud database (HighChem LLC, 2013-2021) for comparing MS² spectra. If a compound had at least one positive match with the predicted compound in either database as well as a peak quality score above 8 in the reserved extract, this level 3 (L3) or higher tentative candidate was selected to be used for calculating its effective Henry's law constant (K_H , mol Pa⁻¹ m⁻³). These properties were predicted using the HENRYWINTM model as part of the EPI SuiteTM package which provides the values at 298 K (US EPA, n.d.). If the EPI SuiteTM was able to find an experimental value based on a CAS lookup match, those values were used over the model



prediction. This is only applicable to the minority of identified species. The effective Henry's law solubility was converted to a dimensionless effective Henry's law constant (H^*) using the equation:

$$H^* = K_H * \bar{R}T \quad (1)$$

175 Where \bar{R} is the ideal gas constant ($8.3144626 \text{ m}^3 \text{ Pa K}^{-1} \text{ mol}^{-1}$) and T is temperature (K). This conversion allows for a dimensionless comparison and considers dissociation and hydration effects. This calculation, however, requires structural information about a compound. As a result, performing this calculation on a L3 tentative structural candidate can be specious or misleading. Regardless, H^* for structural isomers using HENRYWINTM typically differs less than 3 orders of magnitude with an overall average of
180 approximately 1.5. This accuracy is sufficient for this analysis (Isaacman-Vanwertz and Aumont, 2021).

2.3 Retention Calculation and Tracer Corrections

The signals of species that also appeared in the travel blanks were first subtracted from the M-AL samples to remove their ambient signal but remained in the dataset as they exceeded the sample-to-blank
185 ratio of 5 and could not be considered background. A naturally occurring tracer was selected from the dataset for both positive and negative mode to correct for any dilution, evaporation, and desorption that may occur. To be an ideal tracer, the compound should be fully retained during freezing and have an adequate MS signal. For this work, the peak quality was required to be higher than 8 in the reserved extract and for there to be a positive database match for the predicted composition. For negative mode,
190 this tracer was 4-Nitrophenol ($\text{C}_6\text{H}_5\text{NO}_3$, 139.0269 m/z , 9.7 min, L3). This was chosen as previous experiments by Borchers et al., (2024) have identified this compound to have a retention coefficient of 1.01 ± 0.07 during riming experiments, where desorption and evaporation effects are likely to be more influential than in the present experiment due to enhanced ventilation and much smaller droplet size. For positive mode, xylitol ($\text{C}_5\text{H}_{12}\text{O}_5$, 152.0685 m/z , 1.6 min, L3) was selected as the tracer as its H^* has been
195 determined to be higher than 10^8 (Compernelle and Müller, 2014), which according to Borchers et al.,



(2024) and Jost et al., (2017) indicate its retention coefficient can be safely assumed to be 1, even under the higher exchange conditions of wind tunnel experiments. Regardless of the accuracy of the L3-assigned structure, these tracers represent species with retentions very close to 1 that allow for a reference to that value to compare between samples and make corrections for non-freezing mass exchange.

200 The equation for calculating the retention coefficient is adopted from Borchers et al., (2024) and Jost et al., (2017) and used here as

$$R = \frac{S_{\text{substance}}^{\text{sample}} / S_{\text{substance}}^{\text{RES}}}{S_{\text{tracer}}^{\text{sample}} / S_{\text{tracer}}^{\text{RES}}} \quad (2)$$

where the numerator describes the ratio between the peak area of the substance of interest in the ice sample ($S_{\text{substance}}^{\text{sample}}$) and in the reserved extract sample ($S_{\text{substance}}^{\text{RES}}$). The denominator describes the same ratio but for the tracer ($S_{\text{tracer}}^{\text{sample}} / S_{\text{tracer}}^{\text{RES}}$). Since no dilution effects are involved in the measurement and all samples are measured in the same aqueous matrix, signal ratios can be compared directly without a calibration curve, provided that detector response is linear within the given range of measurement. Given that ions below the threshold intensity of linearity were excluded from measurement, dynamic mass calibration of the HRMS was performed prior to measurement, and that HRMS instruments of this generation show linear dynamic ranges of at least five orders of magnitude (Kaufmann and Walker, 2017), it is reasonable to assume linearity over the measurement range. As ventilation and evaporation effects are quite low in the M-AL (Szakáll et al., 2021), their effects are compensated for by the tracer. Compensating for desorption effects is more complex. As desorption is thought to be driven mainly by linear diffusion and thus enhanced by increased ventilation, species with higher than ambient concentrations as well as species with higher vapor pressures are thought to be disproportionately influenced. However, since the M-AL has little ventilation to enhance desorption, HiVol filter sampling already bias against high vapor pressure species (Bidleman et al., 2020), and ambient filter sampling is closer to ambient concentrations relative to previously simulated single component mixtures, desorption

215



effects are only compensated for by the tracer and nonuniform desorption effects are considered
220 negligible.

Further data analysis was performed with MATLAB ver. R2023a. Distribution modeling was performed using the Distribution Fitter from the Statistics and Machine Learning Toolbox 12.5, based on the Stable Distribution and t Location Scale Distribution models provided in *Univariate Stable Distributions* (2020) and *Univariate Continuous Distributions* (2015) (Nolan, 2020; Yee, 2015).

225 3 Results and Discussion

3.1 Dataset Description

In the negative mode, from over 2800 MS features measured, 548 significant, non-background detected compounds were found. 208 met the peak quality constraints and were then used for analysis. 196 compounds (94%) had successfully assigned compositions and 77 were then selected for additional
230 property calculations.

In the positive mode, 342 significant, non-background detected compounds were found from over 1800 features. 250 met the peak quality constraints and were then used for analysis. 218 of those compounds (87%) had successfully assigned compositions. 84 were then selected for additional property calculations. Comparatively fewer compounds were assigned compositions in the positive mode as
235 phosphorous containing species were not considered. These can represent almost a third of positively ionizable species in rainwater WSOC (Seymore et al., 2023) so it likely makes up a significant portion of species variety that is not considered.

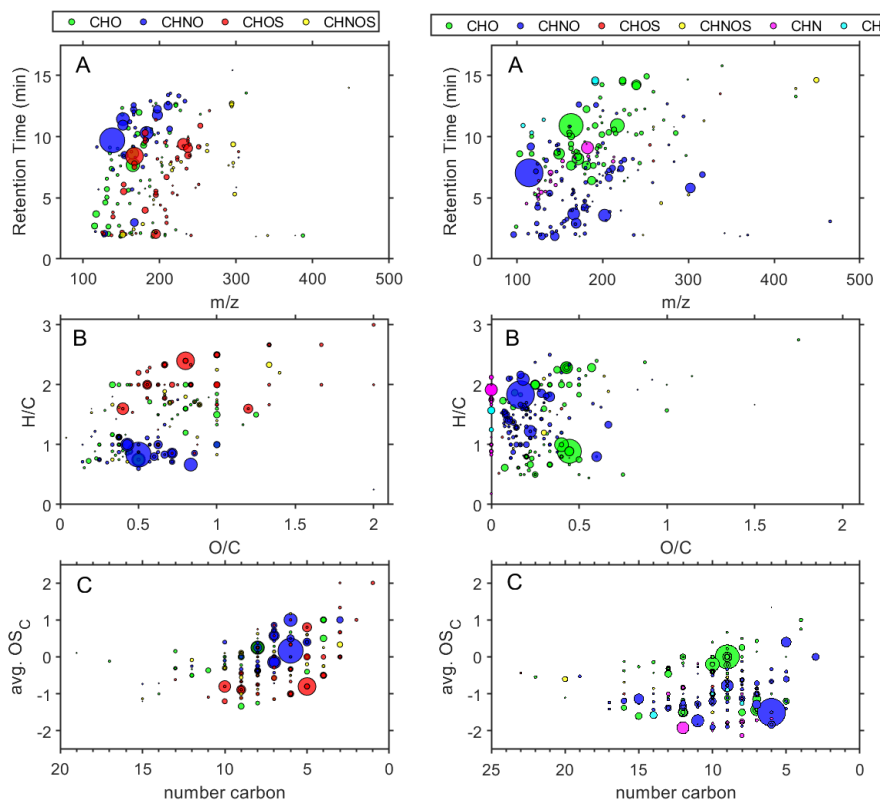


Figure 1. (A) Scatter plot of HPLC Retention time (min) vs m/z ratio; (B) van Krevelen diagram of O/C ratio vs H/C ratio; (C) Kroll diagram of number of C atoms against the average oxidation state of C; Left panels are for negative ionization mode (-)HESI, right panels are positive ionization mode (+)HESI. Area of the marker indicates relative intensity in the reserved extract while color denotes compositional class of the assigned compound: Green for CHO, blue for CHNO, red for CHOS, yellow for CHNOS, magenta for CHN, cyan for CH.

245

Figure 1 illustrates that the dataset is indicative of a typical urban influenced WSOC profile of a dilute sample. In the negative mode, the most significant signals are several nitrophenols and nitroaromatics; notably $C_6H_5NO_3$ (139 m/z , 9.7 min, L3) and $C_6H_4N_2O_5$ (184 m/z , 10.3 min, L3) are



tentatively identified as 4-nitrophenol and 2,4-dinitrophenol respectively. These nitrophenols ionize
250 efficiently in (-)HESI which explains in part their prominence in Figure 1.B where they cluster around
0.6-0.9 H/C and are indications of biomass and fossil fuel burning emissions (Taneda et al., 2004). The
prominent CHOS compounds in the negative mode are alkylorganosulfates, notably $C_5H_{12}O_4S$ (168 m/z ,
8.4 min, L3) and $C_8H_{18}O_4S$ (210 m/z , 12.9 min, L3), which are typical markers of secondary processed
automobile and shipping traffic OM.(Blair et al., 2017; Qi et al., 2021) These can most easily be seen in
255 Figure 1.B above 2 H/C. Some of the other notable CHOS compounds below 2 H/C are terpene-derived
organosulfates such as camphorsulfonic acid ($C_{10}H_{16}O_4S$, 232 m/z , 9.4 min, L2), which also demonstrate
secondary processing under urban conditions (Iinuma et al., 2007; Surratt et al., 2007).

The most significant positive mode signals in Figure 1 come from caprolactam ($C_6H_{11}NO$, 114
 m/z , 7.0 min, L2) and several coumarin derivatives ($C_9H_6O_2$, 146 m/z 7.4 min, L2; $C_9H_8O_4$, 162 m/z , 10.9
260 min, L3; $C_9H_8O_3$, 164 m/z , 8.7 min, L3; $C_{10}H_8O_4$, 192 m/z , 9.0 min, L3). Caprolactam is a cyclic amide
and indicative of industrial emission influence as it is primarily used for manufacturing synthetic fibers
but also used in numerous other manufacturing activities. Caprolactam is a monitored compound on the
hazardous air pollutants list by the United States Environmental Protection Agency (U. S. Environmental
Protection Agency, n.d.). Coumarin species are known brown carbon components and have biomass
265 burning sources as well as potential secondary pathways (Xing et al., 2023).

The several other prominent CHNO compounds are mostly amines, e.g. $C_{11}H_{23}NO_2$ (201 m/z , 3.6
min, L3), $C_9H_{11}NO_2$ (165 m/z , 3.7 min, L3), DL-Stachydrine ($C_7H_{13}NO_2$, 143 m/z , 1.8 min, L2), etc. This
is consistent with known amine-nitrate aerosol formation during winter months where there are sources of
amine salts and semi-volatile organic amine compounds, particularly in areas with high agricultural and
270 combustion emissions (Price et al., 2016). The other prominent CHNO compounds are tentatively
identified as amides such as $C_{12}H_{18}N_2O$ (206 m/z , 6.6 min, L3), $C_{10}H_{14}N_2O$ (178 m/z , 4.2 min, L4),
 $C_3H_4N_4O_2$ (128 m/z , 1.8 min, L3), etc; which can either be further secondary products of AA (Price et al.,
2014) or the result of anthropogenic emissions (Li et al., 2022; Schollée et al., 2017). These amine and



amides tend to have lower retention times and can be seen in the lower cluster in Figure 1.A. The CHO
 275 species present are generally either aromatics or aliphatic acids and separate out as so in the van Krevelen
 diagram in Figure 1.B, with aromatics below 1.5 H/C and acids above such as $C_{12}H_{24}O_3$ (216 m/z , 14.2
 min, L3) and $C_9H_{10}O_3$ (166 m/z , 9.1 min, L3). Very few biogenic CHO species are present as there are
 very few CHO species within 1.5-1.8 H/C that would indicate humics, ligins, or other raw biomass
 markers (Qian et al., 2013). This is consistent with the winter season sampling. Further characterization of
 280 the nonaromatic CHO is difficult to generalize, as there are a variety of sugars, ethers, alcohols, and acids
 that represent various possible biogenic species, terpenoids, and terpene derivatives. For example, xylitol
 (possibly arabitol) ($C_5H_{12}O_5$, 152 m/z , 1.6 min, L3), hexitol ($C_6H_{14}O_6$, 182 m/z , 1.6 min, L3), cinnamic
 acid ($C_9H_8O_2$, 148 m/z , 8.7 min, L3), phthalates such as dimethyl phthalate ($C_{10}H_{10}O_4$, 194 m/z , 10.9 min,
 L2) and phthalic acid ($C_8H_6O_4$, 166 m/z , 7.6 min, L3), as well as succinic acid ($C_4H_2O_3$, 98 m/z , 2.6 min,
 285 L3), levoglucosan ($C_6H_{10}O_5$, 162 m/z , 4.5 min, L2) and farnesol ($C_{15}H_{26}O$, 222 m/z , 14.6 min, L3) are all
 species potentially identified in the dataset.

A few CH and CHN compounds were found only in the positive mode, primarily AA and a couple
 of aromatic hydrocarbons. Combined, these represent less than 11% of the positive mode compounds.
 Only one CHS species was identified ($C_{18}H_{12}S$, 260 m/z , 10.0 min, L4) but was not used for analysis as it
 290 was below peak quality requirements. No CH, CHN, or CHS species were found in the negative mode.

3.2 Retention Coefficients

Table 1. Mean and Median Retention Coefficients by Compound Class and Heteroatom Group

	(-)HESI					(+)HESI				
	Mean	σ	Median	n	n%	Mean	σ	Median	n	n%
Total	0.95	0.21	0.96	208	100	0.95	0.53	0.93	250	100
CHO	0.90	0.25	0.91	68	32.7	1.01	0.82	0.90	73	29.2
CHN	-	-	-	-	-	1.07	0.21	1.04	22	8.8
CHNO	0.96	0.08	0.95	46	22.1	0.94	0.21	0.93	108	43.2



CHNOS	0.97	0.23	0.98	26	12.5	1.11	0.34	0.99	7	2.8
CHOS	0.99	0.23	0.98	56	26.9	0.67	0.59	0.99	3	1.2
CH	-	-	-	-	-	0.66	0.55	0.78	5	2.0
O Containing	0.95	0.21	0.96	196	94.2	0.97	0.54	0.92	191	76.4
N Containing	0.96	0.15	0.96	73	35.1	0.97	0.22	0.95	137	54.8
S Containing	0.99	0.23	0.98	83	39.9	0.98	0.44	0.99	10	4.0

295

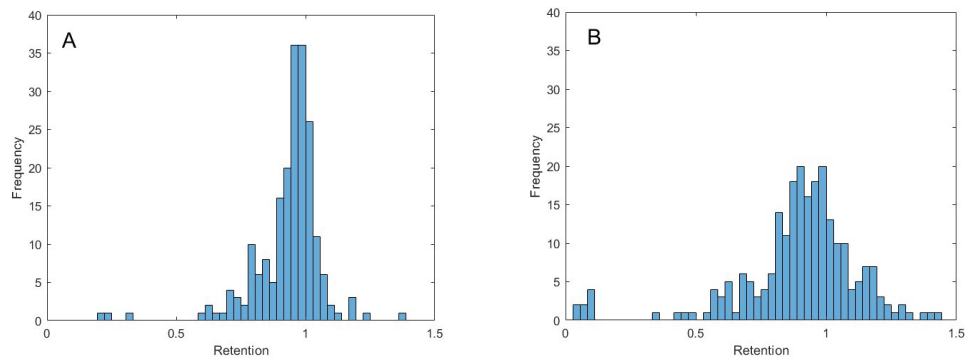


Figure 2. Histograms of Retention Coefficients for all measured L5 and above compounds that met peak quality constraints; (A) (-)HESI, (B) (+)HESI

300

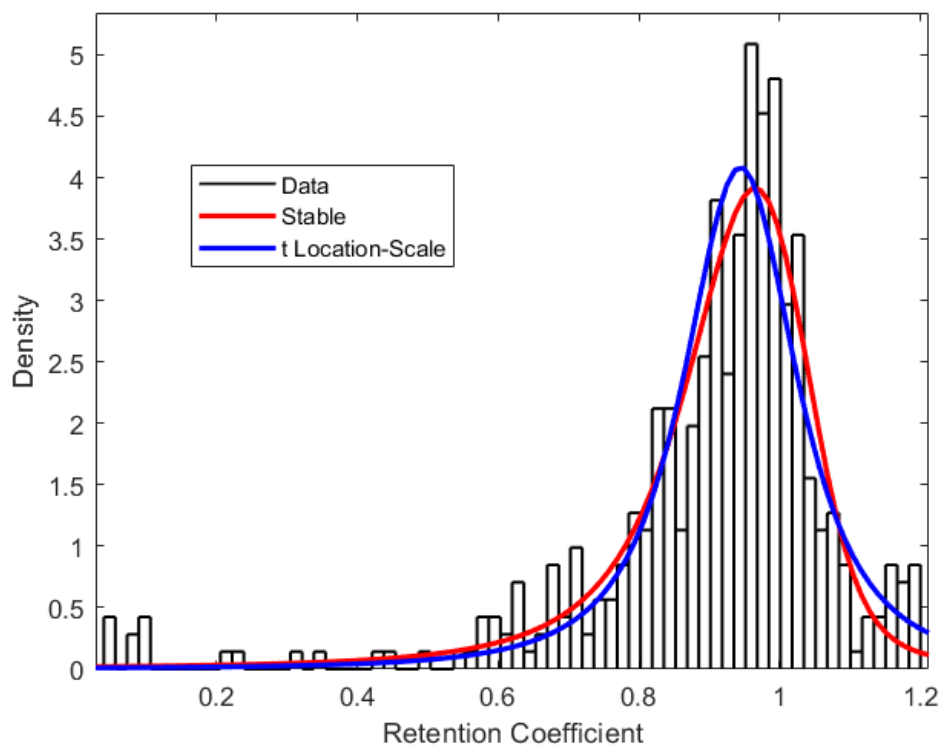


Figure 3. Merged Histogram for (-)HESI and (+)HESI of all Retention Coefficients measured fit with Stable and t Location-Scale distribution parameterizations of statistical density.

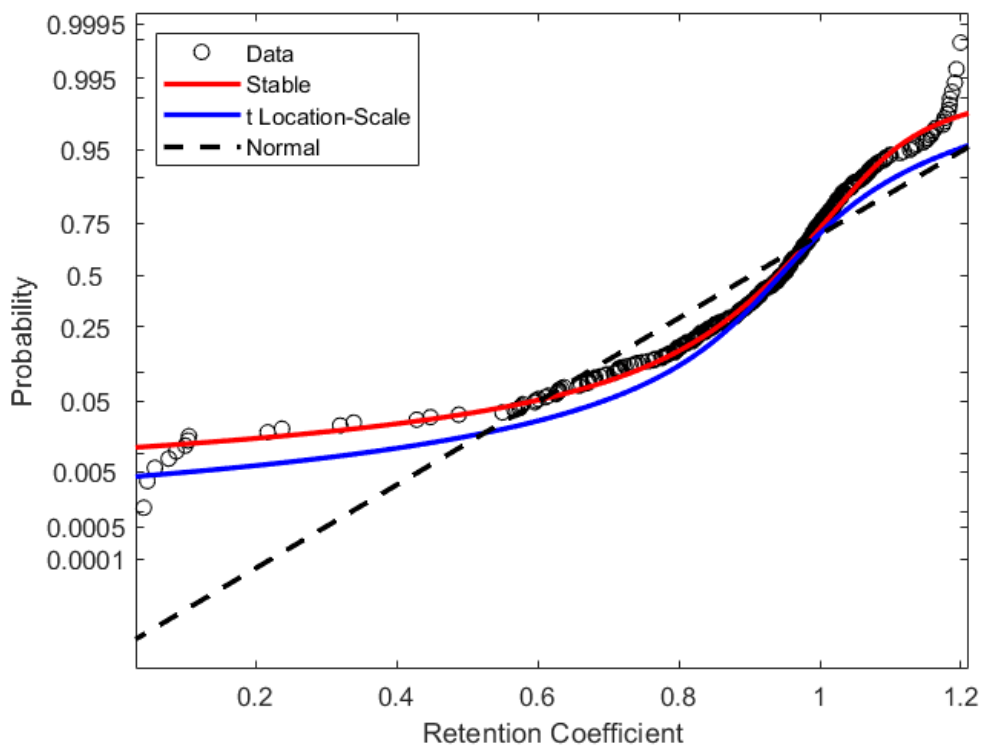
Table 2. Parameters for Stable Distribution Fit presented in Figure 3

Mean	0.8894	
Log Likelihood	224.657	
Parameter	Value	Std. Error
Alpha (α)	1.38642	0.06988
Beta (β)	-0.61652	0.10241
Gamma (γ)	0.07289	0.00383
Delta (δ)	0.95409	0.00608

305

Table 3. Parameters for t Location-Scale Distribution Fit presented in Figure 3

Mean	0.9442	
Log Likelihood	210.775	
Parameter	Value	Std. Error
Mu (μ)	0.94415	0.00566
Sigma (σ)	0.08665	0.00630
Nu (ν)	2.02867	0.26969



310 Figure 4. Probability plot of Retention Coefficients with the Stable and t Location-Scale distribution parameterizations and a Normal distribution

The histograms presented in Figure 2 and Figure 3 illustrate the distribution of retention coefficients determined for this dataset. Each histogram shows a peak at 0.96, 0.93, and 0.94 for (-)HESI, (+)HESI, and the full dataset respectively with average retentions all at 0.95 with standard deviations of 0.21 and 0.53 respectively. These values and the values for each compound class are presented in Table 1. 315 Visually the distributions in Figure 2 appear nonnormal, suggesting a true distribution is being measured. Additionally, Figure 4 shows the data deviates strongly from a normal distribution. Both Shapiro-Wilk and Shapiro-Francia tests indicate nonnormality (p-values: 0.4052, 0.3940 (-)HESI; 0.5698, 0.5611 (+)HESI respectively).



320 Combining these distributions and filtering out outliers, the dataset is fitted with two distributions
to model the dataset: Stable and t Location-Scale. The parameters for these fits can be found in Tables 2
and 3. These distributions are functional estimations of the statistical density of retention coefficients
based on the empirical measurements in this experiment. The Stable distribution appears to model the
data most accurately as the parameter errors are lower than the t Location-Scale and the data points in
325 Figure 4 lie closer to the Stable distribution curve.

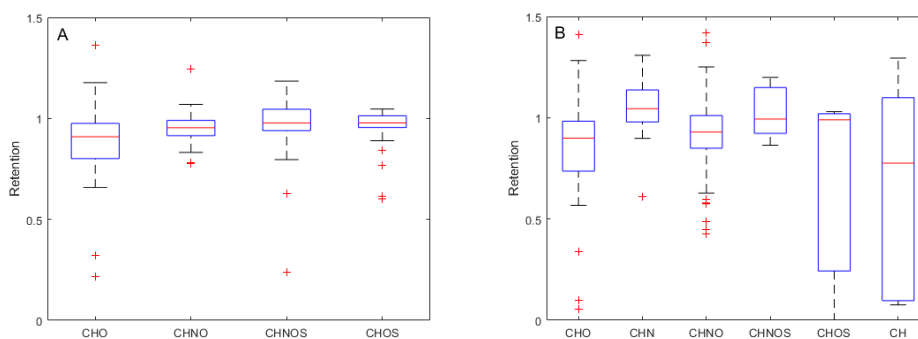


Figure 5. Boxplot of Retention Coefficients by Composition Class; (A) (-)HESI, (B) (+)HESI

330 The means of the composition classes in (-)HESI vary little, generally less than 5% from each
other. In contrast, the means of the composition classes in (+)HESI vary more, up to 40%. The deviations
and ranges of values are also wider in (+)HESI, from 0.21 to 0.82 as seen in Table 1. Visually this can be
seen in Figure 5. For both ionizations, CHNOS tends to be the highest retained along with CHN in
(+)HESI. CHNOS represents more of the heaviest species in the sample set while CHN is entirely AA. In
335 (+)HESI, CHNOS, CHOS, and CH represent the smallest portion of the dataset—less than 6%—and
some of the most variably retained species. For CH, this follows with the variability in hydrocarbon
aqueous solubility, however this variability is more likely explained for CHNOS, CHOS as well with the



smaller sample set bias. Notably, CHO has lower retention with a wider distribution than CHNO in both ionizations. In (-)HESI, CHNO is mostly nitroaromatics while in (+)HESI, CHNO is mostly amines and amides. CHO represents a more similar distribution of organic acids and terpenoids in both positive and negative mode, with more nonpolar species represented in (+)HESI. The lower retention among CHO may then be based on its distribution of organic acids versus terpenoids. This data suggests that nitrate species and amines/amides have similar retentions. It is known that NO_x removal is enhanced by aqueous phase reactions (Daito et al., 2000) and that organic nitrogen represents an important fraction of WSOC (Saxena and Hildemann, 1996; Zhang et al., 2002), but this data may also indicate that nitrogen chemistry on CHO species enhances their retention in hydrometeors. Other UHRMS studies of rainwater have suggested similar explanations for nitrogen uptake in hydrometeors and rainwater organic nitrogen's high bioavailability (Seymore et al., 2023).

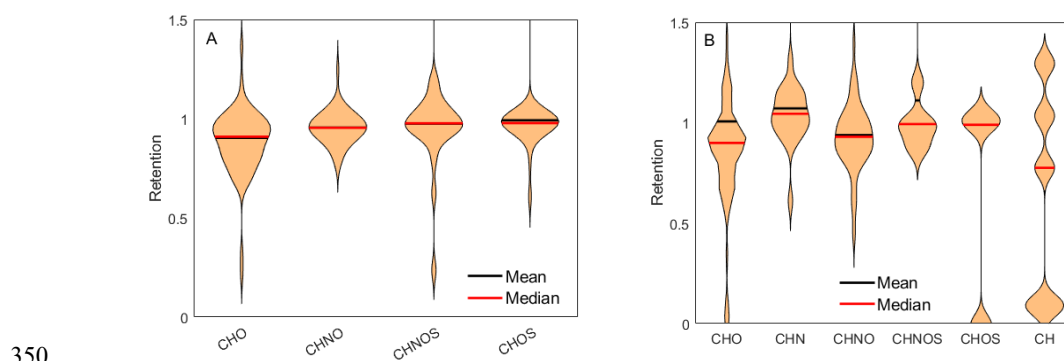


Figure 6. Violin plots of Retention Coefficients by Composition Class; (A) (-)HESI, (B) (+)HESI

The distributions of CHNO and CHOS in (-)HESI seen in Figure 6 show a coincidence of the mean and median along with strong symmetry around the mean. This indicates visually that they appear to be normally distributed, suggesting that the true retentions for the whole of these compound classes may be close to 1. Both Shapiro-Wilk and Shapiro-Francia tests indicate normality (p-values: 0.1920,

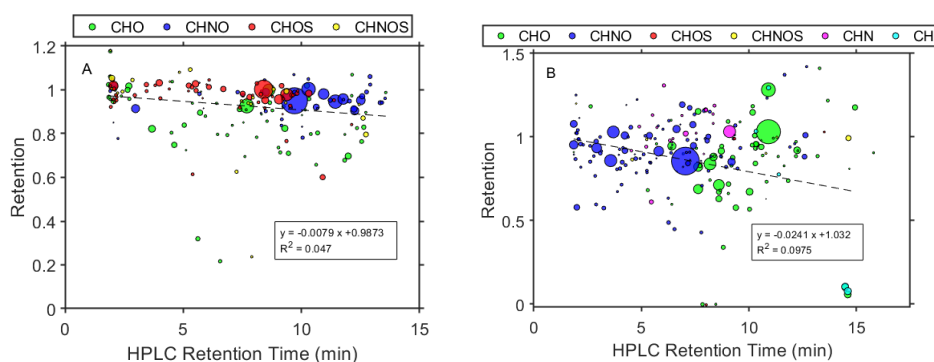


0.1922) for CHNO but not for CHOS (7.7595×10^{-9}). It therefore would be reasonable to assume a normal distribution for CHNO, but CHOS cannot be rigorously stated as normally distributed. CHO and CHNOS show unique distributions with a significant number of values within $-\sigma$ and below, indicating there are certain CHO species that are not retained during freezing.

360 For (+)HESI, the samples sizes for CHNOS, CHOS, and CH are too small to make meaningful descriptions of their distributions. For CHO, CHN, CHNO, the distributions are visually nonnormal and also do not pass any statistical test for normality. The distributions also appear less smooth than their negative mode counterparts, likely a result of previously discussed ionization variability in (+)HESI. Notably, (+)HESI shows a few species with very low retention specifically within the CHO, CHOS, and
365 CH groups. Specifically, these are $C_{14}H_{22}$ (190 m/z , 14.5 min, L3), $C_{15}H_{26}O$ (222 m/z , 14.6 min, L3), and what appears to be a phenyl-sulfide species ($C_{16}H_{18}OS$, 258 m/z , 8.0 min, L4). This is the only identified organosulfide within the dataset. It would be speculative to say that its low retention may indicate that organosulfides as a class are unretained and thus unlikely to appear in the dataset. Its low retention likely has more to do with its low polarity. $C_{14}H_{22}$ and $C_{15}H_{26}O$ as long chain, nonpolar species demonstrate that
370 species with lower aqueous solubilities are also likely to have low retentions.

Concerning heteroatoms, the distributions and ranges of retentions are quite similar among all groups. Oxygen-containing species appear to have a slightly wider distribution which is mostly weighted by the CHO class. Nitrogen-containing species have a smaller standard deviation than the O or S containing species, indicating fewer species with variable retentions and more fully retained compounds. This further
375 suggests that nitrogen inclusion enhances retention (see also Figure S1).

3.3 Correlation of Retention Coefficients with Chemical Properties



380

Figure 7. Retention Coefficient as a function of HPLC Retention time; (A) (-)HESI, (B) (+)HESI; Color denotes compositional class of the assigned compound, as used in Fig. 1: Green for CHO, blue for CHNO, red for CHOS, yellow for CHNOS, magenta for CHN, cyan for CH. Dashed line shows linear fit.

385 The determined molecular weight (MW) shows little correlation linearly with retention (as seen in Figure S2). In (-)HESI, there is a weak positive correlation, suggesting larger compounds are more likely to be retained. This is likely related to lower vapor pressures associated with larger MW species in the negative mode. An F-test against the constant value model indicates that this correlation is not significant (p-value: 0.0857). However in (+)HESI, there's a very weak negative correlation for MW
390 which suggests the opposite. An F-test against the constant value model indicates that this correlation with MW is also not significant (p-value: 0.1440). This trend in the positive mode is likely driven more by polarity, as Figure 1.A also demonstrates that larger species in (+)HESI tend to have higher HPLC retention times and are therefore more nonpolar. The plot in Figure 8 further demonstrates this with a stronger negative correlation between the HPLC retention time and the retention.

395 Figures 7 shows correlations for retention coefficients with HPLC retention time. With reverse-phase HPLC, retention time is a direct proxy for molecular polarity, i.e. shorter retention times indicate higher polarity and longer retention times indicate more nonpolar species. Both (-)HESI and (+)HESI show significant negative correlation between retention and retention time and therefore polarity; an F-



test against the constant value model shows p-values of 0.00193 for (-)HESI and 1.44×10^{-6} for (+)HESI.

400 This indicates that nonpolar species are likely to be unretained and this appears to be especially true for the previously discussed long chain species, such as $C_{14}H_{22}$ (190 m/z , 14.5 min, L3) and $C_{15}H_{26}O$ (222 m/z , 14.6 min, L3) compounds. In Figure 7, a few compound classes separate distinctly by polarity, particularly the CHOS and CHNO in (-)HESI as well as CHO and CHNO in (+)HESI. These polarity differences in these classes may be the driving force in the difference of the retention between CHOS and

405 CHNO in (-)HESI, but unlikely for CHO and CHNO in (+)HESI as CHO spans a much wider range of retentions that cannot be explained solely by polarity.

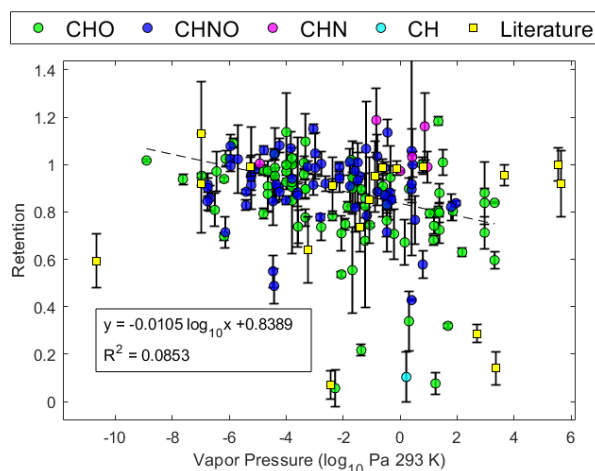


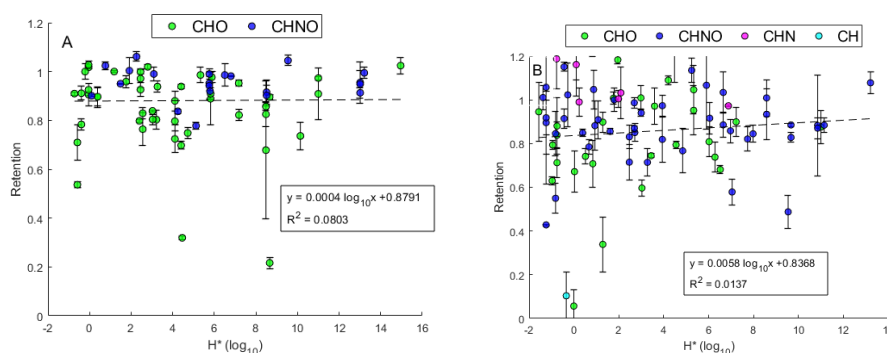
Figure 8. Retention Coefficient as a function of Estimated Vapor Pressure; Color denotes compositional class of the assigned compound: Green for CHO, blue for CHNO, magenta for CHN, cyan for CH, yellow squares for values taken from literature. Dashed line shows linear fit.

410

Further chemical property correlations with retention could be made for the species with estimated chemical properties. The first plot, Figure 8, uses the measured retention coefficient to plot against calculated vapor pressure (VP). It demonstrates a significant negative correlation with VP; an F-



415 test against the constant value model gives a p-value of 1.42×10^{-4} . It is relevant to note that the majority
of species measured are considered semi-volatile (vapor pressure: 10^{-9} to 10 Pa; SVOC) with few low
volatility (LVOC) and intermediate volatility organic compounds (IVOC) (Weschler and Nazaroff, 2008).
LVOC and IVOC are bias against in the sampling method as many LVOCs are highly oxygenated
compounds which may be less sensitive compared to other compounds in UHPLC-Orbitrap MS (Wang et
420 al., 2024) and most IVOCs are revolatilized during sampling (Bidleman et al., 2020). VP is also the
property most associated with desorption effects, likely contributing to some of the negative trend seen in
Figure 8. However, it is mostly associated with IVOC and less with SVOC so desorption alone is not
likely to fully explain this correlation.



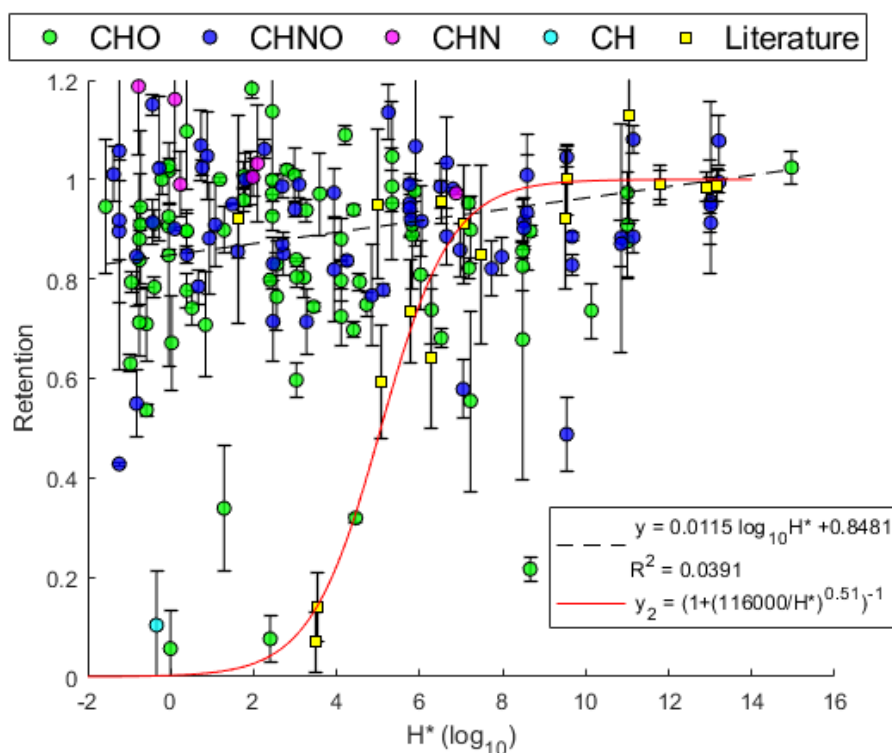
425

Figure 9. Effective Henry's Law Constant H^* versus Retention Coefficient; (A) (-)HESI, (B) (+)HESI; Color denotes compositional class of the assigned compound: Green for CHO, blue for CHNO, magenta for CHN, cyan for CH. Dashed line shows linear fit.

430 Demonstrated in Figure 9, retention shows little or no dependency on H^* under the present
experimental conditions. The linear correlations are not significant for neither (-)HESI or (+)HESI; with
p-values of 0.9270 and 0.3530 respectively for the F-test against the constant value model. The very slight



positive correlation shows agreement with Stuart and Jacobson's (2003, 2004) observation that high H^* species are more likely to be 100% retained but does not show sigmoidal behavior as modeled by Jost et al., 2017 (plotted for reference in Figure 10). This could be the result of differing physical experimental parameters, such as larger droplet size (2 mm versus 20 micron). However, directly comparing the known literature values for retention coefficients with the observations made here does not immediately indicate the systems are incompatible or exclude the comparison.



440 Figure 10. Effective Henry's Law Constant H^* versus Retention Coefficient; Color denotes compositional class of the assigned compound: Green for CHO, blue for CHNO, magenta for CHN, cyan for CH; Yellow squares denote values taken from Borchers et al., (2024), Jost et al., (2017), and Von Blohn et al., (2011, 2013). Dashed line shows linear fit. Solid red line gives the parameterization by Jost et al., (2017).



Figure 10 compares the data presented in Figure 9 against the literature values presented by
445 Borchers et al., (2024), Jost et al., 2017, and Von Blohn et al., (2011, 2013). This comparison does not
appear incongruous, i.e. no discernible difference can be seen between wind tunnel experiments and these
observations. While the measurements presented by Borchers et al., (2024), Jost et al., (2017), and Von
Blohn et al., (2011, 2013) are physically dissimilar experiments to this study—i.e. wind tunnel
experiments, small droplets of micrometer size, high ventilation conditions—their observations are
450 congruent with this experiment. The literature values include only three species with $H^* < 10^4$ and the
lowest H^* of them, pinandiol, is excluded from the parameterization presented by Borchers et al., (2024)
as it was perceived as an outlier. Without more measurements of compounds with $H^* < 10^4$ under wind
tunnel conditions, it is difficult to determine if the nonsigmoidal behavior seen in this experiment is the
result of different physical parameters—specifically the lower surface-to-volume ratio—or if the
455 sigmoidal behavior described by Borchers et al., (2024) and Jost et al., (2017) is an overfit of a limited
dataset. Evidence presented by Gautam et al., (2024) in part 1 of this publication series makes a
compelling case for the dominance of physical parameters at these drop sizes. Critical to these
experiments, Gautam et al., (2024) observed the formation of an ice shell, which inhibited any further
expulsion of dissolved substances during freezing.

460

4 Conclusions

This study presents the measurement of the retention coefficients for real, complex WSOCs from
urban particulate matter for direct drop freezing under raindrop size conditions. The overall distribution of
the retention of WSOCs forms a real, nonnormal distribution up to 1. Looking at the individual
465 compound classes of organics, the data shows that they may have different distributions of
retention coefficients. Most negatively ionizable CHNO and CHOS compounds appear to be fully
retained, indicating that nitroaromatics and organosulphates are favorable to be retained. Slight positive



470 correlations between MW, polarity, and H^* are seen with retention along with a negative correlation with VP. No sigmoidal relationship with H^* was observed. This is likely the result of the lower surface-to-area ratio for this drop size and the ice shell formation observed by Gautam et al., (2024) in part 1 of this publication series. However without further measurements of single component solutions for compounds with $H^* < 10^4$ under wind tunnel conditions, specifically for small cloud droplet sizes, it is difficult to determine if the nonsigmoidal behavior seen in this experiment is solely the result of physical parameters or if the sigmoidal behavior described by other studies is an overfit of a limited dataset.

475 Sulfides, lipids, aromatic hydrocarbons, and long chain compounds are among the most unretained and incidentally the fewest species observed. These are also among the most nonpolar species observed, which is presumably the dominant factor in that regard. CHO species show the highest variability for their measured retentions, most likely related to the distributions of polarity and VPs among the sugars, organic acids, and terpenoids seen here.

480 AA don't follow the trends associated with polarity and VP but are among the most highly retained species. The explanation for this is possibly in its structural properties, which cannot be easily determined using this analytical method. AA solubility in water is largely determined by the dimension and structure of the alkyl substituents, such that AA with longer chains are less soluble than AA with shorter chains and AA with branched substituents are less soluble than AA with linear groups with the same number of carbons (Badocco et al., 2015). Polarity and hydrogen bonding are also known
485 contributors to AA solubility but this is not unique to AA. Hydrogen bonding potential may enhance retention along oxygen functionalities such as among nitro and sulphate species. Hydrogen bonding alone, however, is unlikely to fully explain the high retentions among nitro and sulphate species. Specifically, nitro species have weak hydrogen bonding potential (Shugrue et al., 2016) and as a result is
490 likely influenced mostly by the increased polarity imparted by the nitro substituent or its dissociation.

The data suggests that nitrogen and sulfur inclusion generally increase a species' ability to be retained. Overall, this insulates that the products of NO_x and SO_x reactions from anthropogenic emissions



enhances the retention of these SOA species, reducing the likelihood of reaching the upper atmosphere. Further on this, other studies have demonstrated that NO_x removal is enhanced by aqueous phase reactions (Daito et al., 2000). These findings may also indicate that this NO_x chemistry on CHO species enhances their retention in hydrometeors, potentially by increasing its polarity or solubility. Other UHRMS studies of rainwater have suggested similar explanations for nitrogen uptake in hydrometeors and rainwater organic nitrogen's high bioavailability (Seymore et al., 2023). Additionally, correlations with VP and polarity show that lower VP species and more polar species tend to be retained. Atmospheric chemical processing generally tends to oxidatively degrade large nonpolar species into more water-soluble, less volatile species (Iavorivska et al., 2016). Specifically, aqueous phase droplet chemistry is known to facilitate condensed phase SOA formation from highly volatile species (McNeill, 2015). However, many freshly aged terpene products increase in volatility or see only small decreases in VP with oxidation for their early generation products (Bilde and Pandis, 2001; Kurtén et al., 2018; Wu et al., 2021). This insulates that many freshly oxidized SOA precursors may have a lower potential to be retained than aged organics and may generally suggest that freshly oxidized SOA precursors are more likely to reach the upper atmosphere than primary organics or aged SOA.

The use of UHPLC-HRMS has allowed for the study of ambient WSOC retention rather than single component or limited mixture experiments from previous studies. The experiment in this paper demonstrates the viability of UHPLC-HRMS analysis for ambient WSOC and shows the need for further complex mixture study regarding retention. Future study on retention within hydrometeors should include complex mixture analysis under the physical conditions most similar to the atmosphere, i.e. wind tunnel experiments, smaller droplets, increased ventilation. These studies would also be improved with more distinguishable tracers with known retentions and more sophisticated corrections for desorption. Further studies on single component solutions of species with $H^* < 10^4$ under atmospherically similar physical conditions would also allow for stronger conclusions from the comparison of the retentions measured in this study with other experiments performed under wind tunnel conditions.



The experiment presented here also cannot distinguish between species incorporated within ice crystal structure and those phase-separated but physically constrained to the hydrometeor, potentially
520 between crystal grain boundaries or on the particle surface. That distinction is also not atmospherically relevant regarding the net transport of organics into the upper troposphere. While this method aims to demonstrate the retention for real WSOC, this method is still sample method biased against higher volatility species and likely features other sampling bias typical for HiVol filter based measurements such as filter extraction bias and solvation effects. These measurements also present the distribution of
525 retention coefficients for the variety of species present and not necessarily the mass distribution of species potentially present in the atmosphere. Corrections for species abundancy must first be made in order to apply this data to organic transport models.

Acknowledgements

530 Special thanks to Konstantin Dörholt for his initial work and experimentation in the Mainz Wind Tunnel with these samples.

This work was funded by the Deutsche Forschungsgemeinschaft (DFG, German Research Foundation) – TRR 301 – Project-ID 428312742.

This work was supported by the Max Planck Graduate Center with the Johannes Gutenberg University of
535 Mainz (MPGC).

Author Contributions

JS, MG, MS, AT participated in designing the experiments; LZ provided the samples; JS, JM prepared the samples for experiments; MG performed the experiments; JS, JM, AV conducted the analytical



measurements; JS analyzed the data and wrote the manuscript draft; MG, MS, AT, JM, AV, TH reviewed
540 and edited the manuscript.

Competing Interests

The contact author has declared that none of the authors has any competing interests.

References

- 545 Andreae, M. O., Afchine, A., Albrecht, R., Holanda, B. A., Artaxo, P., Barbosa, H. M. J., Borrmann, S.,
Cecchini, M. A., Costa, A., Dollner, M., Fütterer, D., Järvinen, E., Jurkat, T., Klimach, T., Konemann, T.,
Knote, C., Krämer, M., Krisna, T., Machado, L. A. T., Mertes, S., Minikin, A., Pöhlker, C., Pöhlker, M. L.,
Pöschl, U., Rosenfeld, D., Sauer, D., Schlager, H., Schnaiter, M., Schneider, J., Schulz, C., Spanu, A.,
550 Sperling, V. B., Voigt, C., Walser, A., Wang, J., Weinzierl, B., Wendisch, M., and Ziereis, H.: Aerosol
characteristics and particle production in the upper troposphere over the Amazon Basin, *Atmos. Chem.
Phys.*, 18, 921–961, <https://doi.org/10.5194/acp-18-921-2018>, 2018.
- Andrés Casquero-Vera, J., Lyamani, H., Dada, L., Hakala, S., Paasonen, P., Román, R., Fraile, R., Petäjä,
T., Olmo-Reyes, F. J., Alados-Arboledas, L., Andrés, J., and Vera, C.: New particle formation at urban and
555 high-altitude remote sites in the south-eastern Iberian Peninsula, *Atmos. Chem. Phys.*, 20, 14253–14271,
<https://doi.org/10.5194/acp-20-14253-2020>, 2020.
- Badocco, D., Di Marco, V., Mondin, A., and Pastore, P.: Cyclic voltammetry as a new approach for the
determination of solubility of aliphatic amines in water, *J Chem Eng Data*, 60, 895–901,
<https://doi.org/10.1021/je5009735>, 2015.
- Bardakov, R., Thornton, J. A., Riipinen, I., Krejci, R., and Ekman, A. M. L.: Transport and chemistry of
560 isoprene and its oxidation products in deep convective clouds, *Tellus B Chem Phys Meteorol*, 73, 1–21,
<https://doi.org/10.1080/16000889.2021.1979856>, 2021.
- Bela, M. M., Barth, M. C., Toon, O. B., Fried, A., Ziegler, C., Cummings, K. A., Li, Y., Pickering, K. E.,
Homeyer, C. R., Morrison, H., Yang, Q., Mecikalski, R. M., Carey, L., Biggerstaff, M. I., Betten, D. P.,
565 and Alford, A. A.: Effects of Scavenging, Entrainment, and Aqueous Chemistry on Peroxides and
Formaldehyde in Deep Convective Outflow Over the Central and Southeast United States, *Journal of
Geophysical Research: Atmospheres*, 123, 7594–7614, <https://doi.org/10.1029/2018JD028271>, 2018.
- Bidleman, T. F., Falconer, R. L., and Harner, T.: Particle/Gas Distribution of Semivolatile Organic
Compounds: Field and Laboratory Experiments with Filtration Samplers, *Gas and Particle Phase
Measurements of Atmospheric Organic Compounds*, 39–71, <https://doi.org/10.1201/9781003078340-4>,
570 2020.
- Bilde, M. and Pandis, S. N.: Evaporation rates and vapor pressures of individual aerosol species formed in
the atmospheric oxidation of α - and β - pinene, *Environ Sci Technol*, 35, 3344–3349,
<https://doi.org/10.1021/es001946b>, 2001.



- 575 Blair, S. L., MacMillan, A. C., Drozd, G. T., Goldstein, A. H., Chu, R. K., Paša-Tolić, L., Shaw, J. B.,
Tolić, N., Lin, P., Laskin, J., Laskin, A., and Nizkorodov, S. A.: Molecular Characterization of
Organosulfur Compounds in Biodiesel and Diesel Fuel Secondary Organic Aerosol, *Environ Sci Technol*,
51, 119–127, https://doi.org/10.1021/ACS.EST.6B03304/SUPPL_FILE/ES6B03304_SI_002.XLSX,
2017.
- 580 Von Blohn, N., Diehl, K., Mitra, S. K., and Borrmann, S.: The retention of nitric acid, hydrochloric acid,
and hydrogen peroxide Wind tunnel experiments on the retention of trace gases during riming: nitric acid,
hydrochloric acid, and hydrogen peroxide The retention of nitric acid, hydrochloric acid, and hydrogen
peroxide, *Atmos. Chem. Phys. Discuss*, 11, 17447–17472, <https://doi.org/10.5194/acpd-11-17447-2011>,
2011a.
- 585 Von Blohn, N., Diehl, K., Mitra, S. K., and Borrmann, S.: Wind tunnel experiments on the retention of
trace gases during riming: Nitric acid, hydrochloric acid, and hydrogen peroxide, *Atmos Chem Phys*, 11,
11569–11579, <https://doi.org/10.5194/ACP-11-11569-2011>, 2011b.
- 590 Borchers, C., Seymore, J., Gautam, M., Dörholt, K., Müller, Y., Arndt, A., Gömmer, L., Ungeheuer, F.,
Szakáll, M., Borrmann, S., Theis, A., Vogel, A. L., and Hoffmann, T.: Retention of α -pinene oxidation
products and nitro-aromatic compounds during riming, <https://doi.org/10.5194/egusphere-2024-1443>,
2024.
- Clarke, A. D., Varner, J. L., Eisele, F., Mauldin, R. L., Tanner, D., and Litchy, M.: Particle production in
the remote marine atmosphere: Cloud outflow and subsidence during ACE 1, *Journal of Geophysical
Research Atmospheres*, 103, 16397–16409, <https://doi.org/10.1029/97JD02987>, 1998.
- 595 Clarke, A. D., Eisele, F., Kapustin, V. N., Moore, K., Tanner, D., Mauldin, L., Litchy, M., Lienert, B.,
Carroll, M. A., and Albercook, G.: Nucleation in the equatorial free troposphere: Favorable environments
during PEM-Tropics, *Journal of Geophysical Research Atmospheres*, 104, 5735–5744,
<https://doi.org/10.1029/98JD02303>, 1999.
- Compernelle, S. and Müller, J. F.: Henry's law constants of polyols, *Atmos Chem Phys*, 14, 12815–
12837, <https://doi.org/10.5194/acp-14-12815-2014>, 2014.
- 600 Daito, S., Tochikubo, F., and Watanabe, T.: Improvement of NO_x removal efficiency assisted by aqueous-
phase reaction in corona discharge, *Japanese Journal of Applied Physics, Part 1: Regular Papers and Short
Notes and Review Papers*, 39, 4914–4919, <https://doi.org/10.1143/JJAP.39.4914/XML>, 2000.
- 605 Diehl, K., Debertshäuser, M., Eppers, O., Schmithüsen, H., Mitra, S. K., and Borrmann, S.: Particle
surface area dependence of mineral dust in immersion freezing mode: Investigations with freely
suspended drops in an acoustic levitator and a vertical wind tunnel, *Atmos Chem Phys*, 14, 12343–12355,
<https://doi.org/10.5194/ACP-14-12343-2014>, 2014.
- 610 Dusek, U., Frank, G. P., Hildebrandt, L., Curtius, J., Schneider, J., Walter, S., Chand, D., Drewnick, F.,
Hings, S., Jung, D., Borrmann, S., and Andreae, M. O.: Size matters more than chemistry for cloud-
nucleating ability of aerosol particles, *Science* (1979), 312, 1375–1378,
https://doi.org/10.1126/SCIENCE.1125261/SUPPL_FILE/DUSEK.SOM.PDF, 2006.
- Fofie, E. A., Donahue, N. M., and Asa-Awuku, A.: Cloud condensation nuclei activity and droplet
formation of primary and secondary organic aerosol mixtures, *Aerosol Science and Technology*, 52, 242–
251, https://doi.org/10.1080/02786826.2017.1392480/SUPPL_FILE/UAST_A_1392480_SM6542.PDF,
2018.



- 615 Hallquist, M., Wenger, J. C., Baltensperger, U., Rudich, Y., Simpson, D., Claeys, M., Dommen, J.,
Donahue, N. M., George, C., Goldstein, A. H., Hamilton, J. F., Herrmann, H., Hoffmann, T., Iinuma, Y.,
Jang, M., Jenkin, M. E., Jimenez, J. L., Kiendler-Scharr, A., Maenhaut, W., McFiggans, G., Mentel, T. F.,
620 Monod, A., Prévôt, A. S. H., Seinfeld, J. H., Surratt, J. D., Szmigielski, R., and Wildt, J.: The formation,
properties and impact of secondary organic aerosol: Current and emerging issues, *Atmos Chem Phys*, 9,
5155–5236, <https://doi.org/10.5194/acp-9-5155-2009>, 2009.
- Heitto, A., Wu, C., Aliaga, D., Blacutt, L., Chen, X., Gramlich, Y., Heikkinen, L., Huang, W., Krejci, R.,
Laj, P., Moreno, I., Sellegri, K., Velarde, F., Weinhold, K., Wiedensohler, A., Zha, Q., Bianchi, F.,
Andrade, M., Lehtinen, K. E. J., Mohr, C., and Yli-Juuti, T.: Analysis of atmospheric particle growth
625 based on vapor concentrations measured at the high-altitude GAW station Chacaltaya in the Bolivian
Andes, *Atmos. Chem. Phys*, 24, 1315–1328, <https://doi.org/10.5194/acp-24-1315-2024>, 2024.
- Iavorivska, L., Boyer, E. W., and DeWalle, D. R.: Atmospheric deposition of organic carbon via
precipitation, *Atmos Environ*, 146, 153–163, <https://doi.org/10.1016/j.atmosenv.2016.06.006>, 2016.
- Iinuma, Y., Müller, C., Berndt, T., Böge, O., Claeys, M., and Herrmann, H.: Evidence for the existence of
organosulfates from β -pinene ozonolysis in ambient secondary organic aerosol, *Environ Sci Technol*, 41,
630 6678–6683, https://doi.org/10.1021/ES070938T/SUPPL_FILE/ES070938TSI20070723_080104.PDF,
2007.
- Iribarne, J. V. and Pyshnov, T.: The effect of freezing on the composition of supercooled droplets—I.
Retention of HCl, HNO₃, NH₃ and H₂O₂, *Atmospheric Environment. Part A. General Topics*, 24, 383–
387, [https://doi.org/10.1016/0960-1686\(90\)90118-7](https://doi.org/10.1016/0960-1686(90)90118-7), 1990.
- 635 Isaacman-Vanwertz, G. and Aumont, B.: Impact of organic molecular structure on the estimation of
atmospherically relevant physicochemical parameters, *Atmos. Chem. Phys*, 21, 6541–6563,
<https://doi.org/10.5194/acp-21-6541-2021>, 2021.
- Jost, A., Szakáll, M., Diehl, K., Mitra, S. K., and Borrmann, S.: Chemistry of riming: The retention of
organic and inorganic atmospheric trace constituents, *Atmos Chem Phys*, 17, 9717–9732,
640 <https://doi.org/10.5194/ACP-17-9717-2017>, 2017.
- Kaufmann, A. and Walker, S.: Comparison of linear intrascan and interscan dynamic ranges of Orbitrap
and ion-mobility time-of-flight mass spectrometers, *Rapid Communications in Mass Spectrometry*, 31,
1915–1926, <https://doi.org/10.1002/RCM.7981>, 2017.
- Kurtén, T., Hyttinen, N., Louise D’Ambro, E., Thornton, J., and Prisle, N. L.: Estimating the saturation
645 vapor pressures of isoprene oxidation products C₅H₁₂O₆ and C₅H₁₀O₆ using COSMO-RS, *Atmos
Chem Phys*, 18, 17589–17600, <https://doi.org/10.5194/acp-18-17589-2018>, 2018.
- Lamb, D. and Verlinde, J.: *Physics and Chemistry of Clouds*, Cambridge University Press, 275–414 pp.,
<https://doi.org/10.1017/CBO9780511976377>, 2011.
- Li, J., Gao, X., He, Y., Wang, L., Wang, Y., and Zeng, L.: Elevated emissions of melamine and its
650 derivatives in the indoor environments of typical e-waste recycling facilities and adjacent communities
and implications for human exposure, *J Hazard Mater*, 432,
<https://doi.org/10.1016/J.JHAZMAT.2022.128652>, 2022.
- Li, Y., Pöschl, U., and Shiraiwa, M.: Molecular corridors and parameterizations of volatility in the
chemical evolution of organic aerosols, *Atmos Chem Phys*, 16, 3327–3344, <https://doi.org/10.5194/ACP-16-3327-2016>, 2016.



- Liu, J., Zhang, F., Xu, W., Sun, Y., Chen, L., Li, S., Ren, J., Hu, B., Wu, H., and Zhang, R.: Hygroscopicity of Organic Aerosols Linked to Formation Mechanisms, *Geophys Res Lett*, 48, <https://doi.org/10.1029/2020GL091683>, 2021.
- 660 Liu, Z., Yim, S. H. L., Wang, C., and Lau, N. C.: The Impact of the Aerosol Direct Radiative Forcing on Deep Convection and Air Quality in the Pearl River Delta Region, *Geophys Res Lett*, 45, 4410–4418, <https://doi.org/10.1029/2018GL077517>, 2018.
- McNeill, V. F.: Aqueous organic chemistry in the atmosphere: Sources and chemical processing of organic aerosols, *Environ Sci Technol*, 49, 1237–1244, <https://doi.org/10.1021/es5043707>, 2015.
- Nolan, J. P.: Univariate Stable Distributions, <https://doi.org/10.1007/978-3-030-52915-4>, 2020.
- 665 Price, D. J., Clark, C. H., Tang, X., Cocker, D. R., Purvis-Roberts, K. L., and Silva, P. J.: Proposed chemical mechanisms leading to secondary organic aerosol in the reactions of aliphatic amines with hydroxyl and nitrate radicals, *Atmos Environ*, 96, 135–144, <https://doi.org/10.1016/J.ATMOSENV.2014.07.035>, 2014.
- 670 Price, D. J., Kacarab, M., Cocker, D. R., Purvis-Roberts, K. L., and Silva, P. J.: Effects of temperature on the formation of secondary organic aerosol from amine precursors, *Aerosol Science and Technology*, 50, 1216–1226, <https://doi.org/10.1080/02786826.2016.1236182>, 2016.
- Qi, L., Zhang, Z., Wang, X., Deng, F., Zhao, J., and Liu, H.: Molecular characterization of atmospheric particulate organosulfates in a port environment using ultrahigh resolution mass spectrometry: Identification of traffic emissions, *J Hazard Mater*, 419, 126431, <https://doi.org/10.1016/J.JHAZMAT.2021.126431>, 2021.
- 675 Qian, K., Kumar, A., Patil, K., Bellmer, D., Wang, D., Yuan, W., and Huhnke, R. L.: Effects of Biomass Feedstocks and Gasification Conditions on the Physicochemical Properties of Char, *Energies* 2013, Vol. 6, Pages 3972–3986, 6, 3972–3986, <https://doi.org/10.3390/EN6083972>, 2013.
- 680 Riva, M., Chen, Y., Zhang, Y., Lei, Z., Olson, N., Chelmo, H. B., Narayan, S., Yee, L., Green, H., Cui, T., Zhang, Z., Baumann, K., Fort, M., Edgerton, E., Budisulistiorini, S., Rose, C., Ribeiro, I., Oliveira, R. e., Santos, E. dos, Machado, C., Szopa, S., Zhao, Y., Alves, E., Sá, S. de, Hu, W., Knipping, E., Shaw, S., Junior, S. D., Souza, R. de, Palm, B., Jimenez, J., Glasius, M., Goldstein, A., Pye, H., Gold, A., Turpin, B., Vizuete, W., Martin, S., Thornton, J., Dutcher, C., Ault, A., and Surratt, J.: Rising Importance of Organosulfur Species for Aerosol Properties and Future Air Quality, <https://doi.org/10.26434/CHEMRXIV.7597397.V1>, 2019.
- 685 Saxena, P. and Hildemann, L. M.: Water-Soluble Organics in Atmospheric Particles: A Critical Review of the Literature and Application of Thermodynamics to Identify Candidate Compounds, *J Atmos Chem*, 24, 57–109, 1996.
- 690 Schollée, J. E., Schymanski, E. L., Stravs, M. A., Gulde, R., Thomaidis, N. S., and Hollender, J.: Similarity of High-Resolution Tandem Mass Spectrometry Spectra of Structurally Related Micropollutants and Transformation Products, *J Am Soc Mass Spectrom*, 28, 2692–2704, https://doi.org/10.1007/S13361-017-1797-6/ASSET/IMAGES/LARGE/JS8B05447_0005.JPEG, 2017.
- 695 Schymanski, E. L., Jeon, J., Gulde, R., Fenner, K., Ruff, M., Singer, H. P., and Hollender, J.: Identifying small molecules via high resolution mass spectrometry: Communicating confidence, *Environ Sci Technol*, 48, 2097–2098, https://doi.org/10.1021/ES5002105/ASSET/IMAGES/LARGE/ES-2014-002105_0001.JPEG, 2014.



- 700 Seymore, J., Felix, J. D., Abdulla, H., Bergmann, D., Campos, M. L. A. M., and Florêncio, J.: Pandemic-Related Anthropogenic Influences on the Dissolved Organic Matter Chemical Character in São Paulo State Wet Deposition by Ultrahigh-Resolution Mass Spectrometry, *ACS Earth Space Chem*, 7, 1929–1946, <https://doi.org/10.1021/acsearthspacechem.3c00076>, 2023.
- Shugrue, C. R., Defrancisco, J. R., Metrano, A. J., Brink, B. D., Nomoto, R. S., and Linton, B. R.: Detection of weak hydrogen bonding to fluoro and nitro groups in solution using H/D exchange, *Org Biomol Chem*, 14, 2223–2227, <https://doi.org/10.1039/C5OB02360B>, 2016.
- 705 Snider, J. R., Montague, D. C., and Vali, G.: Hydrogen peroxide retention in rime ice, *Journal of Geophysical Research: Atmospheres*, 97, 7569–7578, <https://doi.org/10.1029/92JD00237>, 1992.
- Stuart, A. L. and Jacobson, M. Z.: A timescale investigation of volatile chemical retention during hydrometeor freezing: Nonrime freezing and dry growth riming without spreading, *Journal of Geophysical Research: Atmospheres*, 108, <https://doi.org/10.1029/2001JD001408>, 2003.
- 710 Stuart, A. L. and Jacobson, M. Z.: Chemical retention during dry growth riming, *Journal of Geophysical Research: Atmospheres*, 109, <https://doi.org/10.1029/2003JD004197>, 2004.
- Sun, H., Li, X., Zhu, C., Huo, Y., Zhu, Z., Wei, Y., Yao, L., Xiao, H., and Chen, J.: Molecular composition and optical property of humic-like substances (HULIS) in winter-time PM_{2.5} in the rural area of North China Plain, *Atmos Environ*, 252, 118316, <https://doi.org/10.1016/j.atmosenv.2021.118316>, 2021.
- 715 Surratt, J. D., Kroll, J. H., Kleindienst, T. E., Edney, E. O., Claeys, M., Sorooshian, A., Ng, N. L., Offenberg, J. H., Lewandowski, M., Jaoui, M., Flagan, R. C., and Seinfeld, J. H.: Evidence for organosulfates in secondary organic aerosol, *Environ Sci Technol*, 41, 517–527, <https://doi.org/10.1021/ES062081Q/ASSET/IMAGES/LARGE/ES062081QF00006.JPEG>, 2007.
- Szakáll, M., Debertshäuser, M., Philipp Lackner, C., Mayer, A., Eppers, O., Diehl, K., Theis, A., Kumar Mitra, S., and Borrmann, S.: Comparative study on immersion freezing utilizing single-droplet levitation methods, *Atmos Chem Phys*, 21, 3289–3316, <https://doi.org/10.5194/acp-21-3289-2021>, 2021.
- 720 Taneda, S., Mori, Y., Kamata, K., Hayashi, H., Furuta, C., Li, C., Seki, K. I., Sakushima, A., Yoshino, S., Yamaki, K., Watanabe, G., Taya, K., and Suzuki, A. K.: Estrogenic and anti-androgenic activity of nitrophenols in diesel exhaust particles (DEP), *Biol Pharm Bull*, 27, 835–837, <https://doi.org/10.1248/BPB.27.835>, 2004.
- 725 U. S. Environmental Protection Agency: Caprolactam - EPA Health Effects Notebook for Hazardous Air Pollutants, n.d.
- US EPA: EPI Suite™-Estimation Program Interface | US EPA, <https://www.epa.gov/tsca-screening-tools/epi-suite-estimation-program-interface#citing>.
- 730 Wang, K., Zhang, Y., Tong, H., Han, J., Fu, P., Huang, R. J., Zhang, H., and Hoffmann, T.: Molecular-Level Insights into the Relationship between Volatility of Organic Aerosol Constituents and PM_{2.5} Air Pollution Levels: A Study with Ultrahigh-Resolution Mass Spectrometry, *Environ Sci Technol*, 58, 7947–7957, <https://doi.org/10.1021/acs.est.3c10662>, 2024.
- 735 Weigel, R., Borrmann, S., Kazil, J., Minikin, A., Stohl, A., Wilson, J. C., Reeves, J. M., Kunkel, D., De Reus, M., Frey, W., Lovejoy, E. R., Volk, C. M., Viciani, S., D'amato, F., Schiller, C., Peter, T., Schlager, H., Cairo, F., Law, K. S., Shur, G. N., Belyaev, G. V., and Curtius, J.: Atmospheric Chemistry and Physics In situ observations of new particle formation in the tropical upper troposphere: the role of clouds and the



- nucleation mechanism, *Atmos. Chem. Phys.*, 11, 9983–10010, <https://doi.org/10.5194/acp-11-9983-2011>, 2011.
- 740 Weschler, C. J. and Nazaroff, W. W.: Semivolatile organic compounds in indoor environments, *Atmos Environ*, 42, 9018–9040, <https://doi.org/10.1016/J.ATMOSENV.2008.09.052>, 2008.
- Williamson, C. J., Kupc, A., Axisa, D., Bilsback, K. R., Bui, T. P., Campuzano-Jost, P., Dollner, M., Froyd, K. D., Hodshire, A. L., Jimenez, J. L., Kodros, J. K., Luo, G., Murphy, D. M., Nault, B. A., Ray, E. A., Weinzierl, B., Wilson, J. C., Yu, F., Yu, P., Pierce, J. R., and Brock, C. A.: A large source of cloud condensation nuclei from new particle formation in the tropics, *Nature* 2019 574:7778, 574, 399–403, 745 <https://doi.org/10.1038/s41586-019-1638-9>, 2019.
- Wu, R., Vereecken, L., Tsiligiannis, E., Kang, S., Albrecht, S. R., Hantschke, L., Zhao, D., Novelli, A., Fuchs, H., Tillmann, R., Hohaus, T., Carlsson, P. T. M., Shenolikar, J., Bernard, F., Crowley, J. N., Fry, J. L., Brownwood, B., Thornton, J. A., Brown, S. S., Kiendler-Scharr, A., Wahner, A., Hallquist, M., and Mentel, T. F.: Molecular composition and volatility of multi-generation products formed from isoprene 750 oxidation by nitrate radical, *Atmos Chem Phys*, 21, 10799–10824, <https://doi.org/10.5194/acp-21-10799-2021>, 2021.
- Xing, C., Wan, Y., Wang, Q., Kong, S., Huang, X., Ge, X., Xie, M., and Yu, H.: Molecular Characterization of Brown Carbon Chromophores in Atmospherically Relevant Samples and Their Gas-Particle Distribution and Diurnal Variation in the Atmosphere, *Journal of Geophysical Research: Atmospheres*, 128, e2022JD038142, <https://doi.org/10.1029/2022JD038142>, 2023. 755
- Yee, T. W.: Univariate Continuous Distributions, 343–370, https://doi.org/10.1007/978-1-4939-2818-7_12, 2015.
- Zhang, Q., Anastasio, C., and Jimenez-Cruz, M.: Water-soluble organic nitrogen in atmospheric fine particles (PM_{2.5}) from northern California, *Journal of Geophysical Research: Atmospheres*, 107, AAC 3-1, <https://doi.org/10.1029/2001JD000870>, 2002. 760
- Zheng, G., Wang, Y., Wood, R., Jensen, M. P., Kuang, C., McCoy, I. L., Matthews, A., Mei, F., Tomlinson, J. M., Shilling, J. E., Zawadowicz, M. A., Crosbie, E., Moore, R., Ziemba, L., Andreae, M. O., and Wang, J.: New particle formation in the remote marine boundary layer, *Nature Communications* 2021 12:1, 12, 1–10, <https://doi.org/10.1038/s41467-020-20773-1>, 2021. 765